Environ Monit Assess (2021) 193:848
https://doi.org/10.1007/s10661-021-09642-6

Land use/land cover and climate change interaction in the derived savannah region of Nigeria

Akinlabi O. Akintuyi · Mayowa J. Fasona · Amidu O. Ayeni · Alabi S. O. Soneye

Received: 23 February 2021 / Accepted: 20 November 2021

Abstract The interaction of land use/land cover (LULC) and climate change, to a large extent, involves anthropogenic activities. This study was carried out in the derived savannah of Nigeria, a delicate, transition ecological zone between the rainforest and savanna zones where the interaction of LULC and climate change could be well appreciated. Using the remote sensing and GIS, Land Change Modeler (LCM), and multivariate geostatistics tools, the study evaluated coupled interaction between LULC and climate change and assessed the changes in the land use/land cover patterns for the periods 1972, 1986, 2002, and 2019. It also evaluated the present (1941–2019) and future (2020–2050) variability in rainfall patterns and made an attempt to predict the interaction between LULC and climate change in future climate. The results suggest that the urban (built-up) area, waterbody, woodland, and farmland experienced a rapid increase of about 2,400%, 583%, 277%, and 32%, respectively, while the forest cover lost about 39% between 1972 and 2019. Furthermore, the study predicted 46% and 29% reduction in the forested area between 2002 and 2050 and 2019 and 2050, respectively. The study concludes that rainfall will be the major driver of LULC change within the study area under a future climate.

Keywords Land Change Modeler (LCM) · Land use · Remote Sensing · Cramer's V · Rainfall · GIS

Introduction

Global changes in arid, semi-arid, and dry subhumid areas are not necessarily driven by climatologically induced variables. Rather, they are triggered by anthropogenic activities in an attempt by man to adjust to his needs and aspirations (Matthews, 1983). Although the increase in the concentration of greenhouse gases in the atmosphere is the best-known impact of human activities on climate change, land use/land cover (LULC) change may be of equal importance (Pielke, 1997; Pitman et al., 2000). Thus, a basic understanding of the characteristics of climatic parameters and atmospheric conditions over a place for some periods of time would provide an understanding of the significance of LULC changes to climatic variability and change. Large-scale LULC change modifies the surface albedo and surface–atmosphere energy exchanges (Pielke & Avissar, 1990). Consequently, it has an effect on the atmospheric flux of carbon dioxide (CO_2) and determines the contribution of evapotranspiration to the precipitation recycling, which has impacts on both the local, regional, and global climate.

A. O. Akintuyi (✉) · M. J. Fasona · A. O. Ayeni · A. S. O. Soneye
Department of Geography, University of Lagos, Akoka-Yaba, Lagos, Nigeria
e-mail: aakintuyi@unilag.edu.ng

Published online: 27 November 2021

The interaction between LULC and climate is complex (Dale, 1997; Oliver & Morecroft, 2014; Olson et al., 2008) and it can be viewed from three dimensions. First, the interaction of LULC (more specifically vegetation) on climate — LULC induce changes in climate of a region as it is a factor of climate (Fan et al., 2015; Kirtiloglu et al., 2016; Mutiibwa et al., 2014; Orhan et al., 2014). Second, the interaction of climate on LULC or vegetation – change in climate induced LULC change or modifies LULC of a place being an effect of climate (Pielke et al., 2007). Finally, it can be viewed from the feedbacks from the interaction. To this end, most studies have emphasized the interaction of LULC on regional climate and considered LULC as a factor of climate (Dale, 1997; Deng et al., 2013; Xiong et al., 2014). Previous studies in Africa have either not fully integrated or have downplayed the importance of LULC change to climate and climate variability. Also, focus has largely been on the landscape or land fragmentation and vegetation distribution, without any consideration for the human impacts (Pielke, 1997; Pielke et al., 2007; Yaqian et al., 2018). In few instances where LULC were integrated to model scenarios, emphasis has been on the global or regional scale and at a coarse resolution (Pitman et al., 2000; Sohl et al., 2012; Wang et al., 2004; Zeng et al., 1999). For example, Zheng and Eltahir (1997) modeled the response of the West Africa monsoon to deforestation and desertification at horizontal and vertical resolutions of about 2° and 1 km, respectively.

LULC characteristics in Nigeria are closely linked to vegetation distribution and are controlled by the interaction of the variables of climate, soils, and human activities. The Nigeria savannah zone is prone to desert encroachment, increasing temperature and decreasing rainfall, increasing human and animal population, overgrazing, and lack of rangeland for grazing. These have predisposed the area to the dangers of environmental change which include climate change. For instance, changes in land cover patterns are one way in which the effects of climate change are expressed (Dale, 1997). Other ways are land degradation, drought, and flooding, such as the flood experience in substantial parts of Nigeria in 2012, 2014, and 2020. In addition to these problems, are the downward spread of desert encroachment and reducing farm yield, and land conflict between cattle herders from the Sudan and Sahel savannah zones and local farmers of the guinea savannah zone. These have acted as the push factors for the local human and animal population to migrate southward to the derived savannah, an interphase between the more humid southern rainforest zone and drier norther savannah zone, which they consider to be more habitable and conducive because of longer rainy season.

Consequently, the ecological balance of the derived savannah has come under threat as could be seen in recent events within the area. Fasona and Omojola (2005) revealed that 35% of the conflicts reported between 1991 and 2005 within the zone are land resources driven. More recent conflicts between the Fulani pastoralists and arable crop farmers driven by land and water resources have heightened insecurity across several states in the more humid guinea and derived savannah. This scenario may be attributed to the downward movement of nomads from the main savannah zone for greener pasture for their cattle. They have turned this zone to their permanent abode as they are found grazing animals all year round. This situation has provoked the local farmers because the activities of the nomads have affected or compounded their economic problems and reduced food production by destroying or reducing returns from their farm holdings. Nomads' activities also have an effect on the land surface characteristics as farmers have resulted to shifting cultivation, shortened bush fallowing, or deforestation (Geist & Lambin, 2004) to increase their farm holdings. In addition, Ayeni et al., (2013a, b) and Ayeni et al. (2015) assessed the impact of land use/land cover and global changes on water resources in the derived savannah of Nigeria and it was found that forest lost more area to built-up, cultivation, and waterbodies through urbanization, farming, and dam construction. The studies observed that land use and climate changes have the potential to influence rates of runoff and thereby increasing the risk of flooding and evaporation. Therefore, more urbanized areas are likely to experience higher runoff and rates of evaporation, whereas cultivated areas will be susceptible to more infiltration and less surface flow, meaning lower runoff coefficients (Ayeni et al., 2013a, b, 2015; Cook & Vizy, 2006). It was further discovered that Fasona and Omojola (2005); Ayeni et al., (2013a, b) and (2015) did not consider change interactions between land use, climatic variables, and other variables (human) within the period studied. This change interaction, therefore, forms

the gap which this study aims to address since it involved large influence of anthropogenic activities. This study, therefore, evaluates coupled interaction between LULC and climate change for the period between 1972 and 2019. It also assesses the present (1941–2019) and future (2020–2050) variability in rainfall patterns and attempt to predict the interaction between LULC and climate change during future climate.

Study area

The study area covers part of the derived savannah region of Nigeria spanning from latitude 7.0° to 8.75°N and longitude 4.25° to 6.0°E. It is about 37,751.91 km^2 in area and covers the present Ekiti State in its entirety and parts of Kwara, Ondo, Oyo, Osun, Kogi, and Edo States (Fig. 1). The area covered in this study extends into the upper part of the forest ecological zone. This is necessary to capture the interactions of land use/land cover change and climate at the fringes of the ecological zone. The derived savannah is a delicate interphase zone that is undergoing continuous encroachment due to the interplay of climate change and anthropogenic activities over time. It is noted that the zone has been encroaching into the rain forest zone due to the continued pressure from both natural and anthropogenic activities (FME, 2004).

The annual mean rainfall decreases from about 1,600 in the south to 1,200 mm in the north around Ondo and Pategi, respectively. The rainfall pattern is influenced by the orography as evident around the southwest of Efon Ridge and other highlands within the region. The derived savannah usually records two-peak rainfall in July and September, and a relative short dry break in August. The annual mean temperature is about 27.8 °C. The temperature anomaly shows a sinusoidal pattern even though the values are

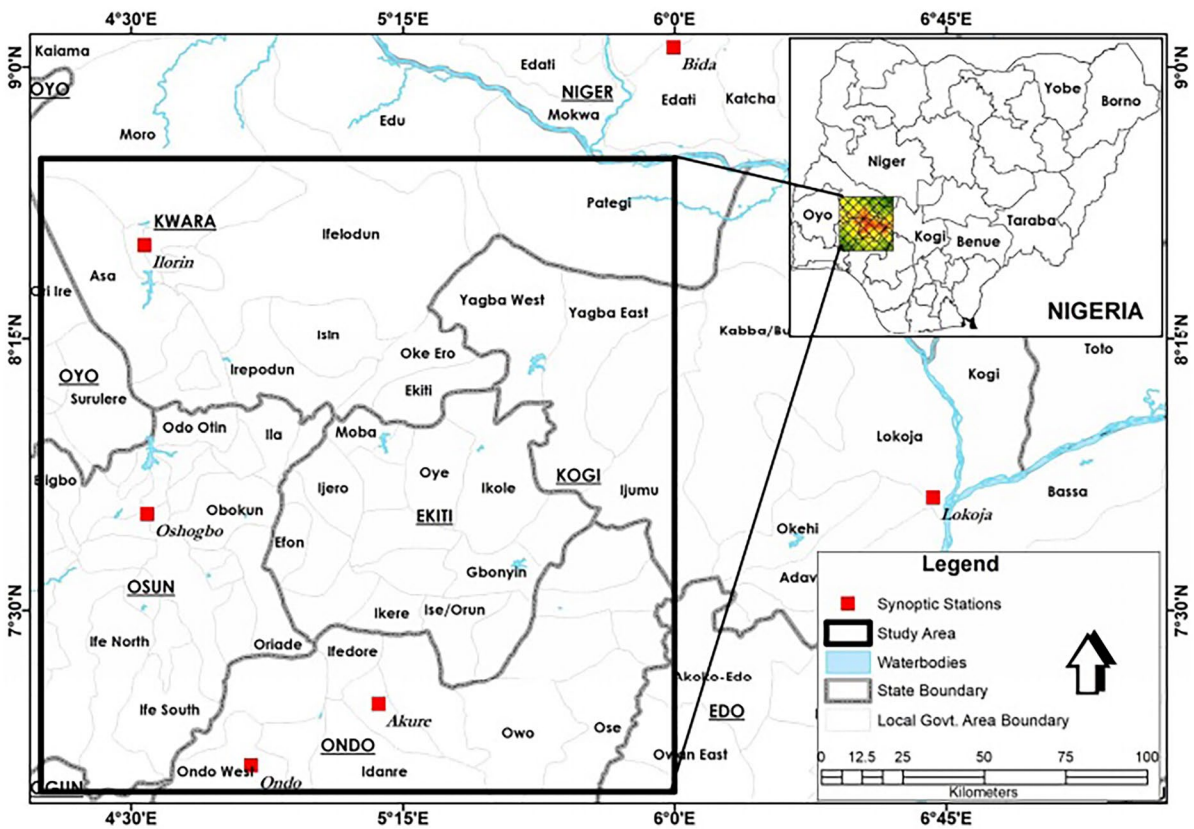

Fig. 1 The study area

relatively high and uniform all the year round. The relief of the area is relatively flat surface, but dominated by ridge system of Fold Mountains, particularly Efon Ridge with elevation ranging from 500 to 900 m above the sea level. Also, the area is well drained by the River Niger and its numerous tributaries, which include Rivers Asa, Osun, Oro, and Awore. Some of these rivers have been dammed for irrigation and domestic water supply.

The population of the study area was estimated to be about 9.8 million generated from 2006 population census of the Federal Republic of Nigeria (NBS, 2006) and projected to 13.6 million in 2019 with an annual growth rate of 3.2%. The area has a population density of 364 persons per square kilometer.

Materials and methods

The methods adopted for the study include the use of remote sensing and GIS, multivariate geostatistical analysis, and spatial modeling techniques as illustrated in Fig. 2.

Data sources and characteristics

The sources and characteristics of spatial data used are presented in Table 1. Specifically, archived series of Landsat data (MSS, TM, and ETM+) for 1972, 1986, and 2002, Landsat 8 (OLI) for 2019, and ASTER DEM covering the study area were sourced from internet portals of the Global Land Cover Facility (GLCF) of Department of Geography, University of Maryland, US Geological Survey Earth Explorer, and Earth Remote Sensing Data Analysis Centre, respectively. The elevation data and other terrain variables (i.e., aspect and slope) were generated from the ASTER GDEM2.

The climatic data (monthly rainfall) for the present (1941 and 2019) and future (2020–2050) climates were obtained from the Nigerian Meteorological Services (NIMET), Lagos and World Climate Research

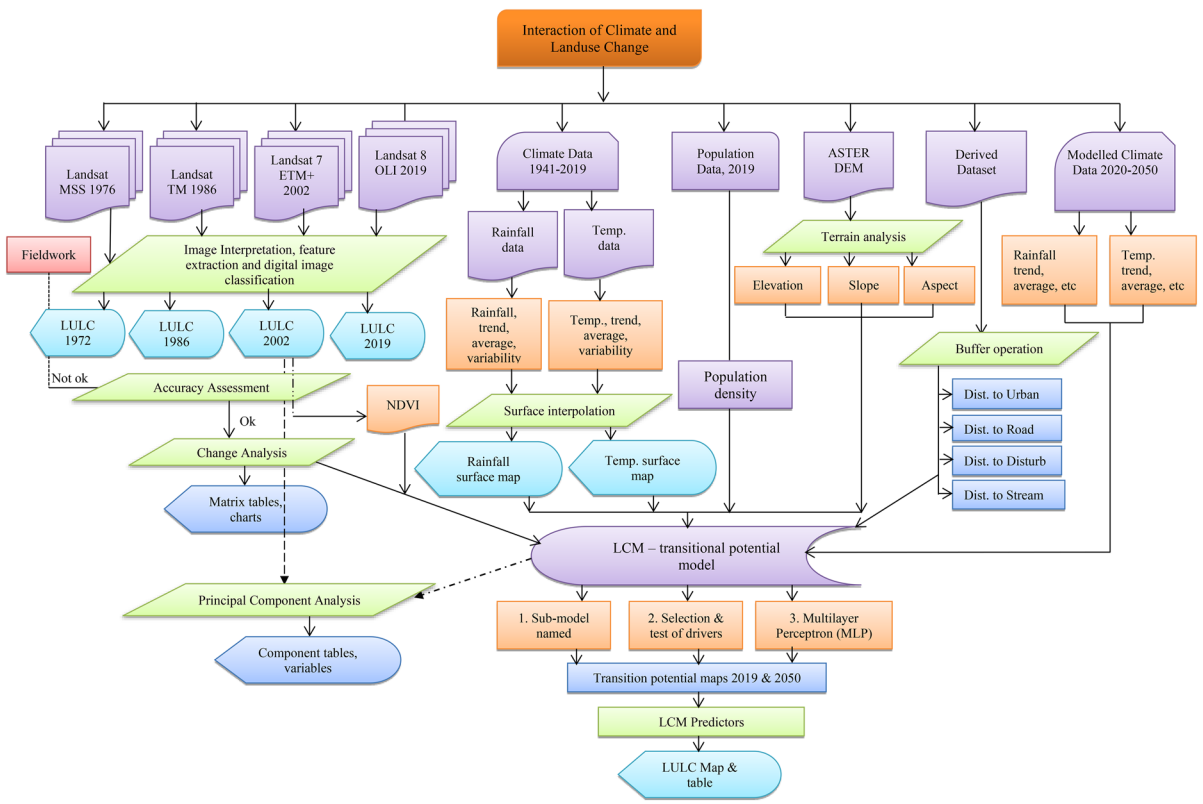

Fig. 2 Research framework

Table 1 Sources and characteristics of data

Data	Identification/coverage	Scale resolution/units	Date	Sources
Landsat 8 OLI Satellite Imagery	Paths 190 and rows 54–55	Spatial & spectral resolutions – 15 (P (0.5–0.68 µm)); 30 m (5 bands – VNIR (0.43–0.88 µm)); 30 m (2 bands – SWIR (1.57–1.65, 2.11–2.29 µm)); 30 m (Cirrus (1.36–1.38 µm)); 100*30 m^2 (2 bands – TIRS (10.60–11.19; 11.50–12.51 µm))	Dec. 2019	USGS Earth Explorer http://earthexplorer.usgs.gov/
Landsat 7 ETM + Satellite Imagery	Paths 190 and rows 54–55	Spatial resolution – 15 (P), 30 m (B-IR), 60 m (TIR); spectral resolution – 8 bands (0.45–2.35 µm, 10.4–12.5 µm)	Nov. 2002	Global Land Cover Facility (GLCF) — www.landcover.org
Landsat TM Satellite Imagery	Paths 190 and rows 54–55	Spatial resolution – 15 (P), 28.5 m (B-IR), 120 m (TIR); spectral resolution – 7 bands (0.45–2.35 µm, 10.4–12.5 µm)	Nov. 1986	Global Land Cover Facility (GLCF) —www.landcover.org
Landsat1 MSS Satellite Imagery	Paths 204–205 and rows 54–55	Spatial resolution – 15 (P), 79 m (G-NIR); spectral resolution – 4 bands (0.5–1.1 µm)	Nov. 1972	Global Land Cover Facility (GLCF) — www.landcover.org
Elevation Data-ASTER GDEM (version 2)	ASTGTM2–(N06E004–N06E006, N07E004–N07006 & N08E006)–9 scenes	Spatial resolution – 30 m or 1 arc second	2011	Earth Remote Sensing Data Analysis Centre www.gds.aster.ersdac.or.jp
Population	Study area	LGA population figure	2006	National Bureau of Statistic (NBS) www.nigerianstat.gov.ng
Future climatic data	Stations–Ilorin, Bida, Lokoja, Akure, Ondo, and Oshogbo	0.5 Degree latitude by longitude	2020–2050	Intercomparison Project phase 3 (CMIP3) (www.engr.scu.edu/~emaurer/global_data/)
Present climatic data	Stations–Ilorin, Bida, Lokoja, Akure, Ondo, and Oshogbo	Rainfall (monthly rainfall) – millimeters (mm)	1941–2019	Nigerian Meteorological Agency (NIMET), Lagos

Programme's (WCRP's) Coupled Model Intercomparison Project phase 3 (CMIP3) multi-model dataset (Meehl et al., 2005), respectively. The study adopted the data from the MRI-CGCM2.3.2 model which simulated and accurately captured the climatology and variability of the West African Monsoon System (Cook & Vizy, 2006). However, there were data gaps in the observed time series data. Nevertheless, the issue of data gaps was resolved by statistically regressing the years with gap against the data of the same period from the nearest station having a similar correlation with the stations with the data gaps. Consequently, the missing years were determined using the trend line equations. Other datasets used for the study were derivatives of the main dataset as presented in Table 1.

Assessment of land use/land cover change

Remote sensing and GIS techniques were used to classify and interpret the satellite images (Landsat MSS, Landsat TM, and ETM+) and to generate the LULC for 1972, 1986, 2002, and 2019. The images used in this current study were acquired in dry season between November and January when the images are cloud free and the possibilities of low classification errors with high spectral contrast between features being investigated. It should be noted that all datasets had already been orthorectified by the providers with a reported root mean square (RMS) errors for positional accuracy of less than 50 m (Tucker et al., 2004). Nevertheless, geometric and radiometric corrections were further performed based on the Armston et al. (2002) and de Vries et al. (2007) methods, respectively. For the classification, we used three reflectance bands for MSS images (1=green, 0.5–0.6 μm; 2=red, 0.6–0.7 μm; 3=near infrared – NIR, 0.7–0.8 μm), three reflectance bands for TM and ETM+(bands 2=green, 0.53–0.61 μm; 4=NIR, 0.76–0.90 μm; and 7=mid infrared – MIR, 2.08–2.35 μm), and three bands (7=shortwave infrared 2 (SWIR 2), 2.11–2.29 μm; 5=NIR, 0.85–0.88 μm; and 3=green, 0.53–0.59 μm) of 12 earth surface reflectance bands of Landsat 8 Operational Land Imager (OLI). This is due to the bands' vibrant shades of green for vegetation and to separate farmland from the different forest stands. The images for each time period were mosaic prior to the classification. The Landsat MSS bands 1, 2, and 3 were used to generate the false color composite image that was interpreted and classified into LULC classes. The bands 2, 4, and 7 of Landsat (TM and ETM+) were used to generate the false color composite images for 1986 and 2002, while bands 3, 5, and 7 were used to generate 2019 image from Landsat 8 OLI. After a careful inspection of the images, eight LULC classes were developed by modifying US Geological Survey Classification System (Campbell & Wynne, 2011) as presented in Table 2. Using the IDRISI Selva software, supervised classification technique based on maximum likelihood algorithm was employed. The training data that correlates with the number of classes were carefully selected, delineated, and subsequently, respective signature files were developed. The maximum likelihood supervised algorithm (defined as MAXLIKE in IDRISI) was used because the selected sample sizes were large enough to permit a clear definition of the training data. The associated Bayesian probability permits combination of mean and variance/co-variance spectral signatures of training data to determine a definite class of that a pixel (Eastman & Laney, 2002; Lark et al., 2017). Consequently, the LULC base maps for 1972, 1986, 2002, and 2019 were generated. The post-classification method (Wright et al., 2013) was adopted for change analysis using the Land Change Modeler (LCM) extension of IDRISI Selva software.

Data validation

The modeling of interaction of LULC and climate change for the future climate was validated using the LULC for 2019 generated from Landsat 8 OLI as the reference map generated and predicted 2019 LULC map. The kappa index (Kno) and Cramer's *V* index of association were calculated using validate algorithm in IDRISI software to compare and check for level of agreement and association in terms of quantity of the LULC classes between the reference and predicted maps.

Evaluation of rainfall variability and change

The monthly rainfall data were summarized and standardized using the combination of annual mean and standard deviation (as in Eqs. 1 and 4), and percentages of coefficient of variation (as shown in Eq. 2) and rainfall variability indices (as shown in Eq. 3) were computed for both the present (1941–2019) and future (2020–2050) climates for all stations using the following formulae:

Table 2 The LULC classification scheme

ID	LULC classes	Description of classes
1	Urban	This covers the built areas, roads, and surfaces with appreciable human constructions
2	Waterbody	This includes all streams, ponds, lakes, dams, and rivers within the study area
3	Forest	Areas covered by broadleaved evergreen and deciduous forest areas of height between 3 and 5 m. It includes wetlands, plantation, and light and heavy, gallery, palm, and montane forests
4	Woodland	This covers areas that were left to fallow after harvesting of forest without any plan to re-grow and where the areas are littered with deadwood
5	Grassland	This covers areas with high to low grasses, shrub, and stunted woods and are used for extensive grazing
6	Farmland	This includes areas covered by all forms of agricultural practices involving tillage and plots with regular and irregular shapes
7	Fire scar	This covers areas with black spots or dots on the imageries that were recognized as bush burning sites for new farmlands
8	Degraded surfaces	This is an area that cannot support plant growth or plant cultivation. It includes exposed surfaces, bare surfaces, and rock outcrops

Modified from USGS Classification System (Campbell & Wynne, 2011)

$$Z = \frac{X - \mu}{\sigma} \quad (1)$$

$$CV = \frac{\sigma}{\mu} * 100 \quad (2)$$

$$\delta_i = (P_i - \mu)/\sigma \quad (3)$$

$$\sigma = \sqrt{\frac{\Sigma(x_i - \mu)}{n - 1}} \quad (4)$$

where Z = anomalies (standardization), CV = coefficient of variation, X = value of climatic variables, δ_i = variability index for year (i), p_i = annual value of the climate parameter for year (i), σ = standard deviation, and μ = mean (Akinsanola & Ogunjobi 2014; Oguntunde et al., 2011).

Single figures were derived for each of the stations and used to create surface maps using the interpolation technique, inverse distance weighted (IDW). The IDW model was adopted to create the surface maps due to irregular space between the synoptic stations within the study area and the influences of phenomena or observations diminish in their contributions with distances. Also, the IDW model interpolates values of observations within the range of data values, so that the approximate values may not contain peaks and valleys. Therefore, as presented in Eq. 5, the IDW involves dividing each of the observations by its distance from the target point raised to a power (α) (Smith et al., 2007). Thus:

$$Z_j = k_j \sum_{i=1}^{n} \left(\frac{1}{d_{ij}{}^{\alpha}} \right) z_i \quad (5)$$

where Z_j = predicted value, d_{ij} = distance between the known value and predicted value, z_i = the known value, and k_j = an adjustment to ensure that the weights add up to 1 (Smith et al., 2007).

Modeling interaction between LULC and climate change

LCM technique was adopted to model the interaction between the LULC and climate change. In using this technique, rainfall was identified as the main underlying and proximate factor of the land use/land cover change in the future climate. Other factors such as population pressure (population density), biophysical factors (nature of terrain, i.e., elevation, aspect, and slope), normalized difference vegetation index (NDVI), and distance from stream, road, and urban centers were identified as catalysts or obstacles to LULC change in certain locations during present climate (Wanga & Davidson, 2007; Hewitson & Crane, 1996; Orhan et al., 2014). However, these factors were considered as static variables for the interaction between LULC and climate during future climate.

The land change prediction in LCM involves three major steps (change analysis, transition potential modeling, and change prediction). Change analysis was performed between LULC maps for 1986 and

2002 and 2002 and 2019 to determine the nature, magnitude, and direction of transition between the LULC classes for present and future climates. Transition potentials modeling involved naming of submodel, test, and selection of variables based on their level of association and importance by considering their Cramer's *V* (i.e., a quantitative measure of association between the variables that ranges from 0 to 1). Variables are selected based on the decision rule that states variables that have a Cramer's *V* of about 0.15 or higher are useful while those with values of 0.4 or higher are good (Eastman, 2012). The Cramer's *V* values for the variables used for this work are presented in Table 3. All variables were suitable, but aspect and distance to stream were rejected due to their low Cramer's *V* values.

Multi-layer perceptron (MLP) used to run the submodel at 10,000 iterations for both present and future climate and transition potential maps were generated thereafter.

Under change prediction tab, transition Markov probabilities were generated based on the transition potential maps. Thereafter, 2019 (present) and 2050 (future) were set for the year of prediction.

Validation and calibration of interaction between LULC and climate change

The predicted interaction between the LULC and climate change within the derived savannah for both present and future climate was validated using kappa index of agreement and Cramer's *V*, a measure of association between the predicted 2019 LULC and as reference data (2019 LULC). Kappa index of agreement values of ≤ 0 indicates no agreement, 0.01–0.20 indicates none to slight agreement, 0.21–0.40 shows fair agreement, 0.41–0.60 shows moderate agreement, 0.61–0.80 specifies substantial agreement, and 0.81–1.00 as almost to perfect agreement (Pontius Jr., 2000). The kappa index of agreement and Cramer's *V* were 0.4507 and 0.4471, which mean there was a moderate agreement and good association between predicted LULC and reference data. The reference data and predicted LULC for 2019 have similar signals pattern as shown in Fig. 3. Therefore, the model simulated LULC patterns for 2019 and 2050 agreed reasonably well as signals and pulses followed a similar trend as could be seen in Fig. 4. However, the computed kappa index and agreement between reference and predicted LULC in terms of quantities and areal characteristics are moderate when they are compared, while the Cramer's *V* of 0.447 showed a strong association between the datasets.

Accuracy assessment

Accuracy assessment was carried out to validate LULC map, 2019 data using error matrix and significance was tested with kappa statistics. A total of 243 points were randomly selected from LULC and compared with Ikonos Image of corresponding area. The errors of omission and commission were determined to be 11% and 11.5% respectively while the overall accuracy was 87.2% (see Table 4). The classification was effective and significant with the kappa statistic value of 69.2%.

Results and discussion

The static LULC patterns

The static characteristics of the land use/land cover generated from satellite imageries for the years 1972, 1986, 2002, and 2019 for the study area of about 37,751.91 km^2 are shown in Fig. 5 and the statistics

Table 3 Cramer's *V* values for the variables

S/n	Explanatory variables (drivers)	Cramer's *V* values	S/n	Explanatory variables (drivers)	Cramer's *V* values
1	Distance to disturbance	0.2502	6	NDVI	0.4441
2	Evidence likelihood	0.4779	7	Distance to stream	0.0508
3	Elevation	0.1527	8	Distance to urban center	0.1355
4	Rainfall (present)	0.2123	9	Distance to road	0.1279
5	Population	0.1962	10	Rainfall (future)	0.2825

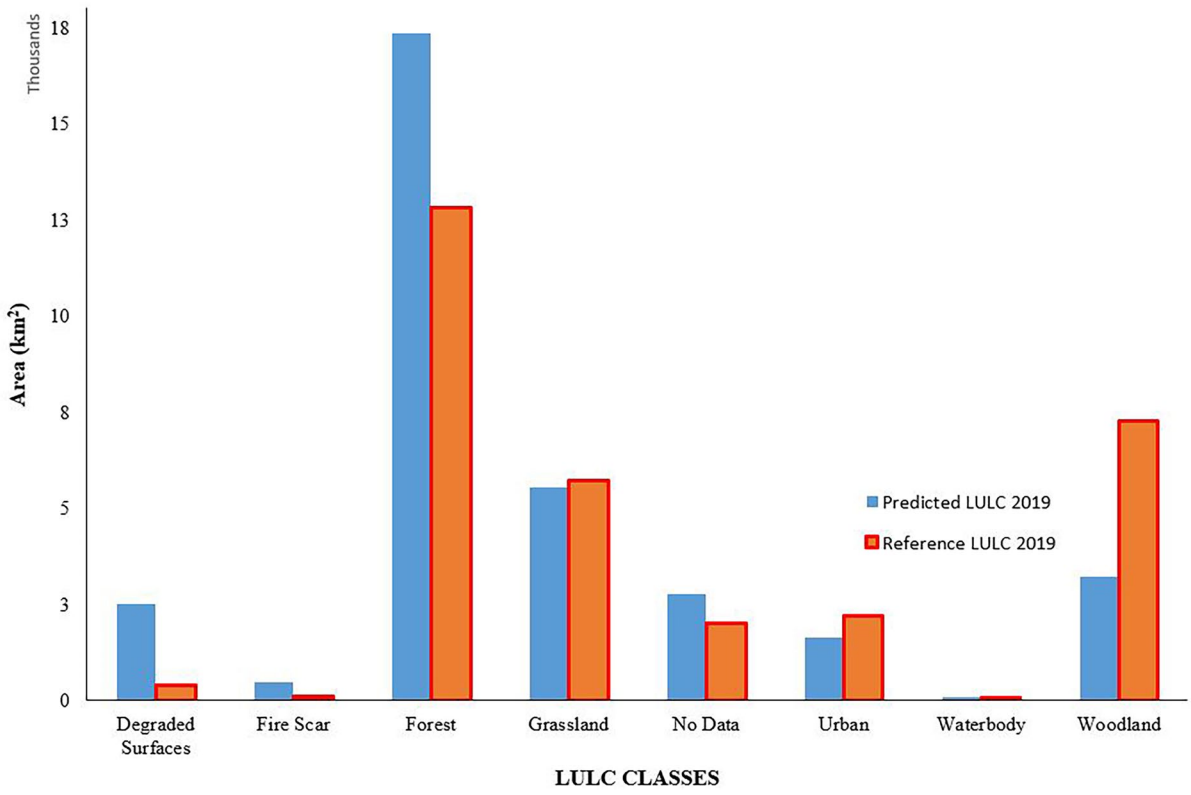

Fig. 3 Comparison of areal characteristics of reference and predicted LULC, 2019

are provided in Table 5. The study revealed that in 1972, there were seven classes of LULC classes within the study area. Degraded surface covered an area of 293.9 km^2, which represents about 0.8% of the total land resources of 37,751.9 km^2. Farmland and forest covered an area of 5,430.5 km^2 and 21,022 km^2, respectively, which account for about 14.4% and 55.7% of the area, while grassland and urban areas occupied about 5,440 km^2 (14.4%) and 88.1 km^2 (0.2%), respectively. In addition, the waterbody and woodland occupied 10.5 km^2 (which is less than 0.0%) and 1,929.7 km^2 (5.1%) respectively as shown in Fig. 5a and Table 5.

In 1986, LULC classes increased to eight with an addition of fire scar. Table 5 illustrated the statistics of the area occupied by the individual LULC classes, while Fig. 5b shows the spatial distribution patterns of the LULC, forest, farmland, grassland, and woodland, which covered about 15,984.1 km^2 (42.3%), 7,419.3 km^2 (19.7%), 5,861.3 km^2 (15.5%), and 3,459.8 km^2 (9.2%), respectively. In addition, the remaining 13.3% of the area was covered by degraded surfaces, fire scar, urban, waterbody, and area without data in the following proportions 345 km^2 (0.9%), 976.1 km^2 (2.6%), 229.1 km^2 (0.6%), 33 km^2 (0.1%), and 3,444.1 km^2 (9.2%), respectively.

In addition, the static characteristics of LULC in 2002 are shown in Fig. 5c and presented statistically in Table 5. The statistics revealed that the study area was covered with 16,959.5 km^2 (44.9%) of forest, 5,559.4 km^2 (14.7%) of woodland, 5,437.5 km^2 (14.4%) of grassland, and 3,828.6 km^2 (10.1%). During the same year, the table also shows that waterbody, urban, degraded surfaces, and fire scar occupied 77.0 km^2, 1,087.4 km^2, 1,479.1 km^2, and 539.8 km^2, respectively, which constitute 0.2%, 2.9%, 3.9%, and 1.4% of the study area. Again, 2,783.7 km^2 (7.4%) comprised area without data or satellite imagery coverage and zero cloud cover was recorded in 2002.

The spatial distribution of LULC of the study area for 2019 is shown in Fig. 5d. The study area was dominated by forest (12,823.1 km^2), woodland

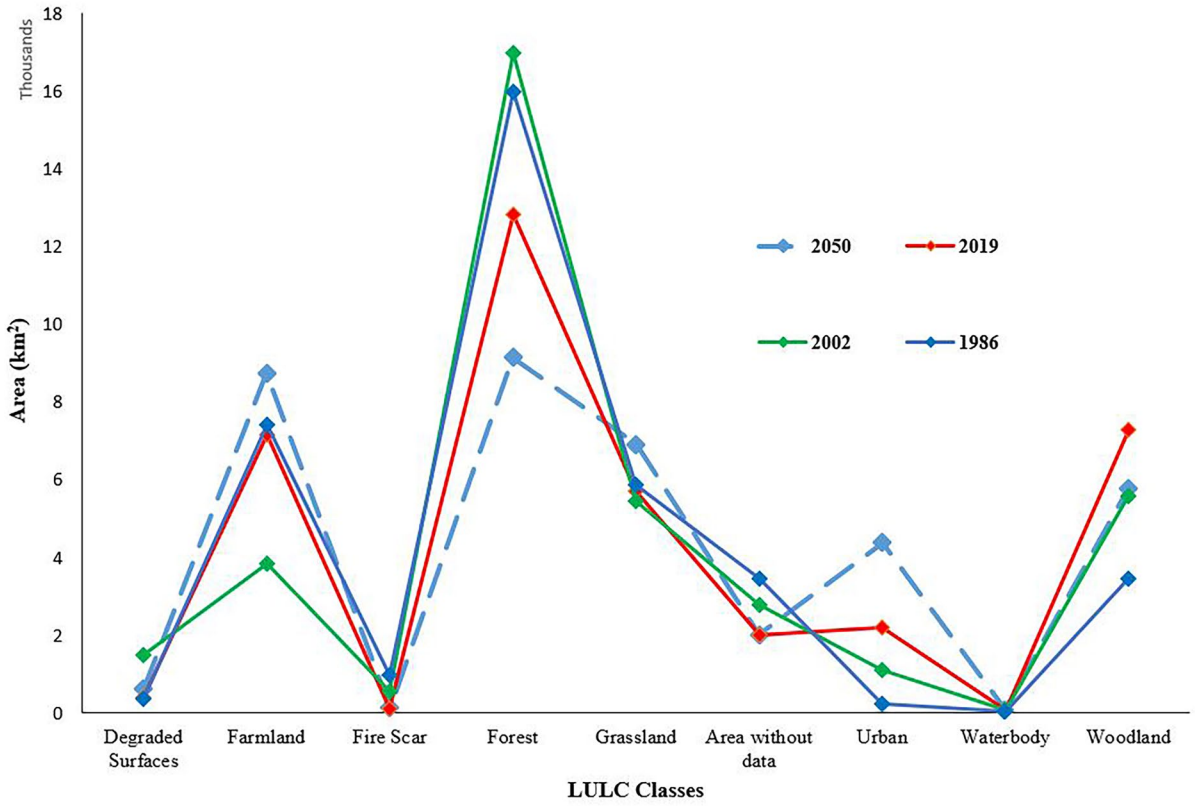

Fig. 4 Agreement between classes of LULC for 1986, 2002, and 2019 and predicted 2050

(7,265.8 km^2), farmland (7,156.6 km^2), and grassland (7,265.8 km^2) which account for about 87% of the total land resources of the area in the order of 34%, 19%, 19%, and 15%, respectively. Also, urban (2,202 km^2) and waterbody (71.9 km^2) covered of about 5.8% and 0.2% respectively as presented in Table 5.

Temporal characteristics of the land use/land cover

The magnitude and nature of change in the static and temporal characteristics of land use/land cover within the study area between 1972 and 2019 are presented in Table 6. The contingency matrices of LULC change for the periods 1972–1986, 1986–2002, 2002–2019, and 1972–2019 are presented in Tables 7, 8, 9, and 10. The study revealed that urban area and farmland gained about 2,400% and 32% of net change between 1972 and 2019. Also, the woodland and waterbody gained 276.5% and 582.5% from 1,929.7 to 7,265.8 km^2 and 10.5 to 71.9 km^2 during the period, respectively. However, forest decreased from 21,022 to 12,823.1 km^2 between 1972 and 2019 by losing about 39% of its total area coverage as presented in Table 6. The study further revealed that grassland demonstrated a sinusoidal nature during the period under study. The grassland gained about 7.7% between 1972 and 1986 and lost about 7.2% by reducing its holding from 5,861 to 5,436 km^2 between 1986 and 2002. In overall, grassland gained 5% between 1972 and 2019 by increasing from 5,437 to 5,717 km^2, which was almost equivalent to the area extent (i.e., 279.5 km^2) gained between 2002 and 2019, which represented 5.1%.

The study showed that grassland, degraded surfaces, farmland, urban, and waterbody gained 7.7%, 17.4%, 36.6%, 160.2%, and 213.3% respectively from their previous locations and area extents to other LULC classes between 1972 and 1986 as presented in Table 6. In addition, Table 7 revealed that grassland, farmland, woodland, and forest lost 70.3%, 68%, 61.4%, and 28.97%, respectively, to other LULC classes between 1972 and 1986. During the same period, degraded surfaces, urban area, farmland, and

Table 4 Accuracy assessment: error matrix analysis for LULC, 2019

LULC	Degraded surface	Farmland	Fire scar	Forest	Grassland	Urban	Waterbody	Woodland	Total	Omission	User accuracy
Degraded surface	**26**	1	2	0	0	2	0	0	31	16.1	83.9
Farmland	0	**28**	1	2	1	0	0	1	33	15.2	84.9
Fire scar	1	0	**18**	1	0	1	0	0	21	14.39	85.7
Forest	0	0	0	**38**	1	0	0	2	41	7.3	92.7
Grassland	0	2	1	1	**22**	0	0	1	27	18.5	81.5
Area without data	0	0	0	0	0	0	0	0	0	0.0	100.0
Urban	3	1	0	0	0	**37**	2	0	43	14.0	86.1
Waterbody	0	0	0	0	0	0	**18**	0	18	0.0	100.0
Woodland	0	1	0	2	1	0	0	**25**	29	13.8	86.21
Total	30	33	22	44	25	40	20	29	**243**	11.0	89.0
Commission error	13.3	15.2	18.2	13.6	12.0	7.5	10.0	13.8	11.5		
Producer accuracy	86.7	84.9	81.8	86.4	88.0	92.5	90.0	86.2	88.5		

waterbody gained more area, which amount to 97%, 81%, 77%, and 75%, respectively. During the period between 1986 and 2002, the study revealed 74.66%, 95.43%, 16.09%, 60.29%, 65.44%, and 71.39% of degraded surfaces, fire scar, forest, grassland, woodland, and farmland recorded were lost to other classes, respectively, while woodland and farmland expanded more to other spatial location and LULC classes by 78.49% and 44.55% as presented in Table 8.

Woodland, urban, grassland, waterbody, and forest gained about 73%, 70%, 64%, 17%, and 11% more to their area extent by encroached into other land uses between 2002 and 2019, respectively. However, during the same period, waterbody, woodland, grassland, farmland, urban, and forest were converted into other land use classes in order of 85%, 65%, 62%, 56%, 39%, and 32% correspondingly as presented in Table 9. Significantly, between 1972 and 2019, it was discovered that farmland, urban, woodland, and waterbody expanded more into other LULC classes by proportions of 72%, 97%, 91%, and 89%, respectively. Also, other major LULC classes like forest and grassland recorded marginal gains of 5.1% and 70.1%, respectively, as presented in Table 10. The urban, waterbody, woodland, and grassland areas expanded annually at 2.1%, 1.9%, 1.9%, and 1.5%, respectively, while the encroachment into forest and woodland areas were at the annual rate of 0.9% and 1.5%, respectively.

Spatial patterns of the present and future rainfall variability

Spatial pattern of present (1941–2019) rainfall variability

The spatial pattern exhibits an increasing trend in the mean annual rainfall towards the southern (i.e., north to south direction) part of the study area during the present climate (1941–2019). The spatial pattern of annual mean rainfall is shown in Fig. 6ai. The mean annual rainfall ranges between 1,208 and 1,662 mm and these extremes were recorded in Ondo and Pategi areas, respectively. Related studies in Nigeria have also predicted similar trend and direction of increasing rainfall (Odjugo, 2011; Oguntunde et al., 2012).

The annual rainfall anomaly recorded during the present climate range between −0.77 and 1.62 which were

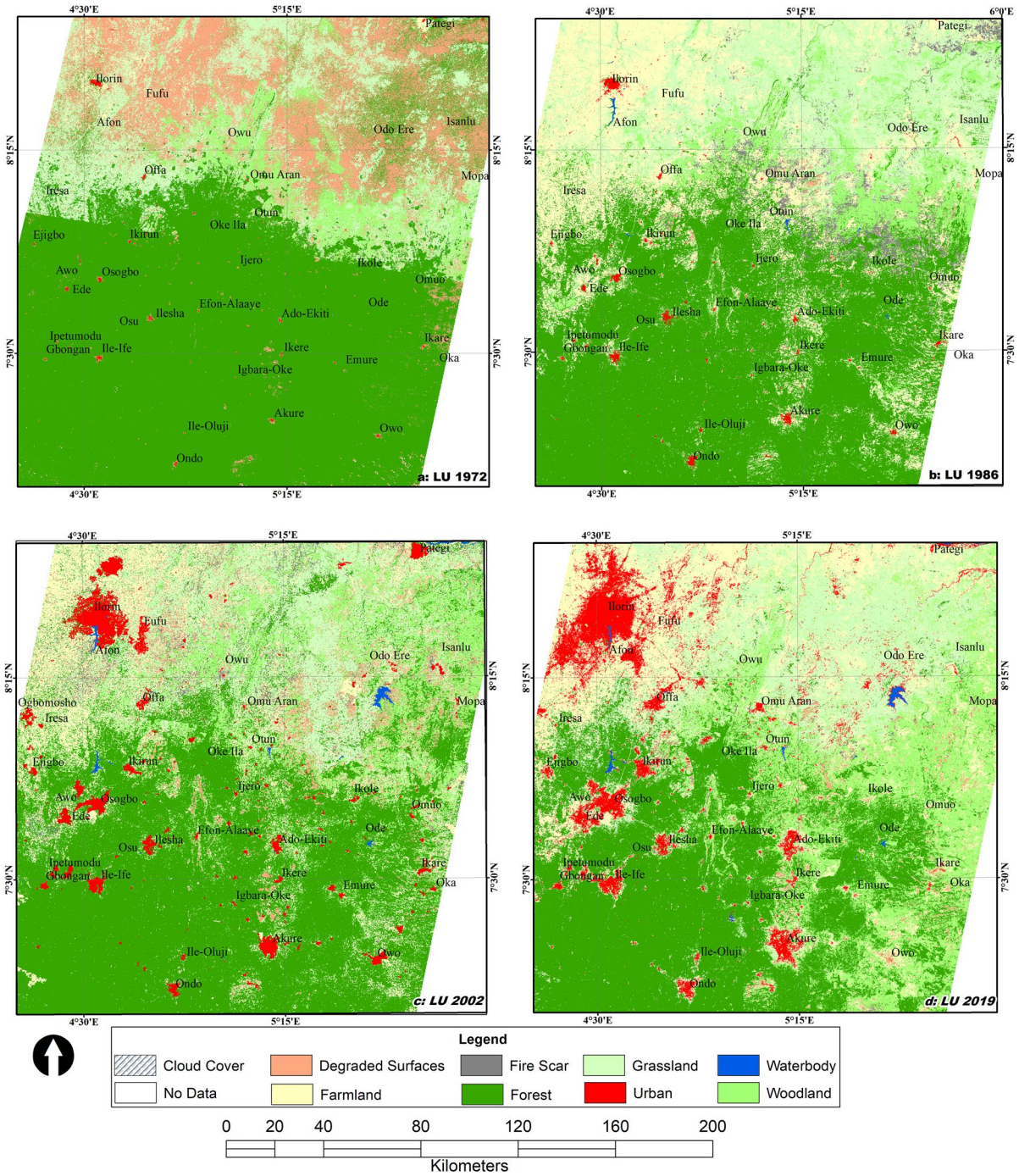

Fig. 5 Spatial distribution of LULC patterns within the study area for **a** 1972, **b** 1986, **c** 2002, and **d** 2019

about 10.5% and 22.1% below and above mean annual rainfall received in the area. Places like Oshogbo, Ilorin, Ogbomosho, Offa, Ede, Isanlu, and Pategi recorded negative rainfall anomaly during the present climate, while Ejigbo, Osu, Ondo, Ado-Ekiti, etc. recorded positive anomaly. The annual rainfall variability indices range from 16 to 26% for the study area during the present climate. In Fig. 6aii, Pategi and Akure recorded

Table 5 Areal extent of static characteristics of the LULC for years 1972, 1986, 2002, and 2019

LULC class	1972		1986		2002		2019	
	Area (km^2)	%	Area (km^2)	%	Area (km^2)	%	Area (km^2)	%
Cloud cover	8.7	0.0	0.1	0.0	0.0	0.0	0.0	0.0
Farmland	5,430.5	14.4	7,419.3	19.7	3,828.6	10.1	7,156.6	19.0
Degraded surface	293.9	0.8	345.1	0.9	1,479.1	3.9	402.8	1.1
Fire scar	0.0	0.0	976.1	2.6	539.8	1.4	105.7	0.3
Forest	21,022.0	55.7	15,984.1	42.3	16,959.5	44.9	12,823.1	34.0
Grassland	5,440.1	14.4	5,861.3	15.5	5,437.5	14.4	5,717.0	15.1
Area without data	3,528.5	9.3	3,444.1	9.1	2,783.7	7.4	2,007.1	5.3
Urban	88.1	0.2	229.1	0.6	1,087.4	2.9	2,202.0	5.8
Waterbody	10.5	0.0	33.0	0.1	77.0	0.2	71.9	0.2
Woodland	1,929.7	5.1	3,459.8	9.2	5,559.4	14.7	7,265.8	19.2
Total	**37,751.9**	**100.0**	**37,751.9**	**100.0**	**37,751.9**	**100.0**	**37,751.9**	**100.0**

least and highest rainfall variability during the present climate. Also, annual rainfall was more stable in areas around Oshogbo, Pategi, Akure, and Ondo which recorded lowest rainfall variability index than 25% recorded in and around Ilorin.

Spatial pattern of future (2020–2050) rainfall variability

The spatial pattern exhibits an increasing trend in the mean annual rainfall towards the southern (i.e., north to south direction) part of the study area during the future climate (2020–2050) as illustrated in Fig. 6bi. The mean annual rainfall ranges between 1,213 and 1,715 mm in the future climate. Pategi will record least amount of rainfall while Ondo will receive the highest mean annual rainfall during the future climate within the study area, which are slightly higher than the values recorded during present climate. The annual rainfall variability indices range from 9 to 13% for the study area during the future climate. Furthermore, there will be a total shift in the distribution of rainfall variability indices in the future climate as captured in Fig. 6bii; Oshogbo and Ilorin will record highest rainfall variability index of 12.9% and 12.7% respectively and Pategi will receive 9.6%.

Land use/land cover and climate change interaction

The static characteristics of the predicted LULC as a result of the interaction LULC and climate change during the present climate are shown in Fig. 7a and the statistics is presented in Table 11. The study revealed that the forest occupies about 17,334.1 km^2, which represents about 46% of the study extent, and grassland, farmland, and woodland cover about 5,534.4 km^2, 4,180.9 km^2, and 3,225.3 km^2, which account for about 15%, 11%, and 9% during the present climate, respectively. The study further revealed that degraded surfaces, urban, and waterbody will take up about 6.6%, 4.3%, and 0.3%, which amount to 2,503 km^2, 1,631 km^2, and 97 km^2 of surface characteristics of the study area in that order were predicted for the present climate.

The study revealed that forest and woodland will occupy about 9,147.4 km^2 and 8,738.4 km^2 which represent about 24% and 23% of the study area respectively during the future climate. Also, grassland, woodland, and urban will cover about 6,907

Table 6 Net change in the land use/land cover (1972–2019)

LULC class	LULC area extent (km^2)				Net change in LULC (km^2)				Percentage change in LULC (%)			
	1972	1986	2002	2019	1972–1986	1986–2002	2002–2019	1972–2019	1972–1986	1986–2002	2002–2019	1972–2019
Cloud cover	8.7	0.1	0.0	0.0	−8.6	−0.1	0.0	−8.7	−99.0	−100.0	0.0	−100.0
Farmland	5,430.5	7,419.3	3,828.6	7,156.6	1,988.9	−,590.8	3,328.0	1,726.1	36.6	−48.4	86.9	31.8
Degraded surface	293.9	345.1	1,479.1	402.8	51.2	1,134.0	−1,076.3	108.9	17.4	328.6	−72.8	37.1
Fire scar	0.0	976.1	539.8	105.7	976.1	−436.2	−434.2	105.7	100.0	−44.7	−80.4	100.0
Forest	21,022.0	15,984.1	16,959.5	12,823.1	−5,037.9	975.4	−4,136.4	−8,198.9	−24.0	6.1	−24.4	−39.0
Grassland	5,440.1	5,861.3	5,437.5	5,717.0	421.2	−423.8	279.5	276.9	7.7	−7.2	5.1	5.1
Area without data	3,528.5	3,444.1	2,783.7	2,007.1	−84.4	−660.4	−776.5	−1,521.4	−2.4	−19.2	−27.9	−43.1
Urban	88.1	229.1	1,087.4	2,202.0	141.1	858.3	1,114.6	2,113.9	160.2	374.6	102.5	2,400.3
Waterbody	10.5	33.0	77.0	71.9	22.5	44.0	−5.2	61.3	213.3	133.5	−6.7	582.5
Woodland	1,929.7	3,459.8	5,559.4	7,265.8	1,530.1	2,099.6	1,706.4	5,336.1	79.3	60.7	30.7	276.5
Total	**37,751.9**	**37,751.9**	**37,751.9**	**37,751.9**	–	–	–	–				

km^2 (18%), 5,762 km^2 (15.3%), and 4.372 km^2 (12%) of 37,751.9 km^2 covered by the entire area correspondingly. Furthermore, degraded surface, fire scar, and waterbody would have expanded to 618 km^2, 123 km^2, and 77 km^2 in 2050, which represent about 1.6%, 0.3%, and 0.2% of the study area as presented in Table 11 and Fig. 7b. In addition, the study revealed that forest area reduced by about 24% from 16,959.53 to 12,823.12 km^2, while the urban area extended by 103% from 1,087.38 to 2,202.01 km^2 of its area coverage in 2019 when compared with the LULC 2002 as presented in Table 12. This can be attributed to the interaction between LULC and climate change during the present climate. During the periods 2019 and 2050, forest and woodland will lose about 29% and 21% respectively to other LULC classes. In all, the study area is predicted to lose about 46% of forest area during the future climate when compared to 2002.

Discussion

Climate has been identified, regionally and globally, as the primary driver of LULCC (Armenteras et al., 2016; Bowman et al., 2009). In this study, we assessed the land use/land cover and climate change interaction to predict the future LULC when the present LULC interacted with the present (1941–2019) and future (2020–2050) climates as presented by the rainfall patterns and other biophysical factors (i.e., terrain, population, distance to disturbance, and stream) in some parts of the derived savannah region of Nigeria. This will facilitate a better understanding of the dynamics of the interaction between LULC and climate change during future climate and provide a basis for land use policies and decision-making on the environment (Fisher et al., 2009; Schirpke et al., 2017). The study showed that the area experienced LULCC and revealed the trend, direction, and location of this change between 1972 and 2019. The built-up area witnessed a rapid increase of about 2,400% from 88.07 to 2,202.01 km^2 between 1972 and 2019. This is due to population increases and the establishment of a new urban area and administration centers arising from the creation of states and local government areas. For example, Osun and Ekiti states were carved out of Oyo and Ondo states in 1991 and 1996, respectively (Omotoso, 2009). Also, waterbody

Table 7 Net change in the land use/land cover, 1972–1986

LULC class	Cloud cover	Degraded surfaces	Farmland	Fire scar	Forest	Grassland	No data	Urban	Waterbody	Woodland	LULC 1972 (km^2)	Loss (km^2)	Loss (%)	Rate (%)
Cloud cover	**0.0**	0.0	0.5	0.0	6.3	0.1	1.5	0.0	0.0	0.3	8.7	8.7	100.0	7.1
Degraded surfaces	0.0	**9.2**	232.8	1.1	6.6	25.4	0.4	16.7	0.6	1.0	293.9	284.6	96.9	6.9
Farmland	0.0	136.6	**1,734.0**	299.5	234.5	2,321.8	178.5	44.6	4.3	476.6	5,430.5	3,696.5	68.1	4.9
Fire scar	0.0	0.0	0.0	**0.0**	0.0	0.0	0.0	0.0	0.0	0.0	0.0	0.0	0.0	0.0
Forest	0.1	54.7	2,944.5	242.0	**14,931.3**	1,222.2	557.4	104.3	10.2	955.4	21,022.0	6,090.7	29.0	2.1
Grassland	0.0	69.3	1,698.8	156.3	531.2	**1,614.5**	115.1	14.6	5.8	1,234.4	5,440.1	3,825.6	70.3	5.0
No data	0.0	33.8	566.1	9.7	137.0	234.8	**2,494.2**	4.4	1.0	47.6	3,528.5	1,034.3	29.3	2.1
Urban	0.0	2.7	31.0	1.8	2.5	3.9	0.5	**42.8**	2.6	0.2	88.1	45.3	51.4	3.7
Waterbody	0.0	0.3	0.2	0.0	0.3	0.1	0.0	1.4	**8.2**	0.0	10.5	2.4	22.5	1.6
Woodland	0.0	38.3	211.5	265.6	134.4	438.5	96.5	0.3	0.3	**744.3**	1,929.7	1,185.4	61.4	4.4
LULC 1986 (km^2)	0.1	345.1	7,419.3	976.1	15,984.1	5,861.3	3,444.1	229.1	33.0	3,459.8	**37,751.9**			
Gain (km^2)	0.1	335.9	5,685.4	976.1	1,052.8	4,246.7	949.9	186.4	24.8	2,715.5				
Gain (%)	100.0	97.3	76.6	100.0	6.6	72.5	27.6	81.3	75.3	78.5				
Rate (%)	7.1	7.0	5.5	7.1	0.5	5.2	2.0	5.8	5.4	5.6				

Table 8 Net change in the land use/land cover, 1986–2002

LULC class	Degraded surfaces	Farmland	Fire scar	Forest	Grassland	No data	Urban	Waterbody	Woodland	LULC 1986 (km^2)	Loss (km^2)	Loss (%)	Rate (%)
Cloud cover	0.0	0.0	0.0	0.0	0.0	0.0	0.0	0.0	0.0	0.1	0.1	99.1	
Degraded surfaces	**87.4**	93.7	11.3	24.2	64.8	12.8	20.7	0.5	29.5	345.1	257.6	74.7	4.7
Farmland	533.4	**2,123.0**	145.6	1,470.7	1,444.5	188.3	625.2	6.5	882.1	7,419.3	5,296.4	71.4	4.5
Fire scar	143.4	74.6	**44.6**	107.1	321.5	0.4	4.3	3.3	276.8	976.1	931.4	95.4	6.0
Forest	111.6	611.6	37.2	**13,411.7**	308.2	17.2	168.3	16.1	1,302.2	15,984.1	2,572.4	16.1	1.0
Grassland	429.1	616.7	209.6	529.2	**2,327.6**	85.1	73.0	16.7	1,574.2	5,861.3	3,533.6	60.3	3.8
No data	38.7	105.3	16.0	431.4	89.7	**2,461.4**	6.4	0.0	295.1	3,444.1	982.6	28.5	1.8
Urban	2.4	25.7	0.6	18.5	4.0	2.7	**170.6**	2.1	2.6	229.1	58.5	25.6	1.6
Waterbody	0.7	1.4	0.9	4.5	0.6	0.0	0.2	**23.6**	1.0	33.0	9.4	28.6	1.8
Woodland	132.4	176.6	73.9	962.2	876.5	15.7	18.5	8.1	**1,195.8**	3,459.8	2,264.0	65.4	4.1
LULC 2002 (km^2)	1,479.1	3,828.6	539.8	16,959.5	5,437.5	2,783.7	1,087.4	77.0	5,559.4	37,751.9			
Gain (km^2)	1,391.6	1,705.6	495.2	3,547.8	3,109.8	322.2	916.8	53.5	4,363.6				
Gain (%)	94.1	44.5	91.7	20.9	57.2	11.6	84.3	69.4	78.5				
Rate (%)	5.9	2.8	5.7	1.3	3.6	0.7	5.3	4.3	4.9				

Table 9 Net change in the land use/land cover, 2002–2019

LULC class	Degraded surfaces	Farmland	Fire scar	Forest	Grassland	No data	Urban	Waterbody	Woodland	LULC 2002 (km^2)	Loss (km^2)	Loss (%)	Rate (%)
Degraded surfaces	**99.7**	511.9	21.0	47.5	371.8	3.7	80.0	0.6	343.0	1,479.1	1,379.4	93.3	5.5
Farmland	49.6	**1,702.9**	9.2	396.5	587.8	57.0	498.9	1.7	524.9	3,828.6	2,125.7	55.5	3.3
Fire scar	12.4	201.6	**3.3**	15.1	169.8	0.7	54.7	1.6	80.8	539.8	536.5	99.4	5.8
Forest	71.9	1,249.3	22.2	**11,472.1**	830.9	16.5	396.9	6.8	2,893.0	16,959.5	5,487.4	32.4	1.9
Grassland	48.6	1,905.3	24.8	129.6	**2,068.7**	12.7	371.0	0.8	876.0	5,437.5	3,368.8	62.0	3.6
No data	32.0	133.5	1.8	120.7	1.9	**1,909.6**	1.1	0.0	583.0	2,783.7	874.0	31.4	1.8
Urban	25.6	317.4	1.2	23.6	32.7	1.7	**664.4**	0.0	20.7	1,087.4	423.0	38.9	2.3
Waterbody	0.2	0.6	0.0	3.3	1.4	0.0	11.7	**59.4**	0.3	77.0	65.3	84.8	5.0
Woodland	62.7	1,134.1	22.1	614.7	1,652.0	5.2	123.3	0.9	**1,944.2**	5,559.4	3,615.2	65.0	3.8
LULC 2019 (km^2)	402.8	7,156.6	105.7	12,823.1	5,717.0	2,007.1	2,202.0	71.9	7,265.8	37,751.9			
Gain (km^2)	303.1	5,453.7	102.4	1,351.0	3,648.3	97.5	1,537.6	12.4	5,321.7				
Gain (%)	75.3	76.2	96.9	10.5	63.8	4.9	69.8	17.3	73.2				
Rate (%)	4.4	4.5	5.7	0.6	3.8	0.3	4.1	1.0	4.3				

Table 10 Net change in the land use/land cover, 1972–2019

LULC class	Degraded surfaces	Farmland	Fire scar	Forest	Grassland	No data	Urban	Waterbody	Woodland	LULC 1972 (km^2)	Loss (km^2)	Loss (%)	Rate (%)
Cloud cover	0.0	0.6	0.0	5.5	0.0	0.0	0.0	0.0	2.5	8.7	8.7	100.0	2.1
Degraded surfaces	**1.9**	147.7	0.1	2.8	29.2	0.0	109.7	0.7	1.8	293.9	146.2	49.8	1.1
Farmland	94.6	**1,977.8**	19.1	112.7	1,837.6	0.0	554.4	16.1	818.3	5,430.5	3,452.7	63.6	1.4
Forest	165.8	2,119.5	42.0	**12,167.6**	1,456.7	0.0	831.2	35.8	4,203.4	21,022.0	8,854.4	42.1	0.9
Grassland	48.6	1,880.3	17.3	290.1	**1,710.5**	0.0	506.3	7.1	979.9	5,440.1	3,729.6	68.6	1.5
No data	35.0	513.5	3.5	205.8	61.3	**2,007.1**	74.4	0.8	627.1	3,528.5	1,521.4	43.1	0.9
Urban	5.0	14.5	0.0	1.1	5.2	0.0	**56.2**	3.3	2.6	88.1	31.8	36.1	0.8
Waterbody	0.0	0.1		0.7	0.1	0.0	1.9	**7.7**	0.0	10.5	2.9	27.2	0.6
Woodland	51.8	502.7	23.6	36.8	616.4	0.0	67.8	0.4	**630.2**	1,929.7	1,299.6	67.3	1.4
LULC 2019 (km^2)	402.8	7,156.6	105.7	12,823.1	5,717.0	2,007.1	2,202.0	71.9	7,265.8	37,751.9			
Gain (km^2)	400.9	5,178.9	105.7	655.6	4,006.5	0.0	2,145.8	64.2	6,635.6				
Gain (%)	99.5	72.4	100.0	5.1	70.1	0.0	97.4	89.3	91.3				
Rate (%)	2.1	1.5	2.1	0.1	1.5	0.0	2.1	1.9	1.9				

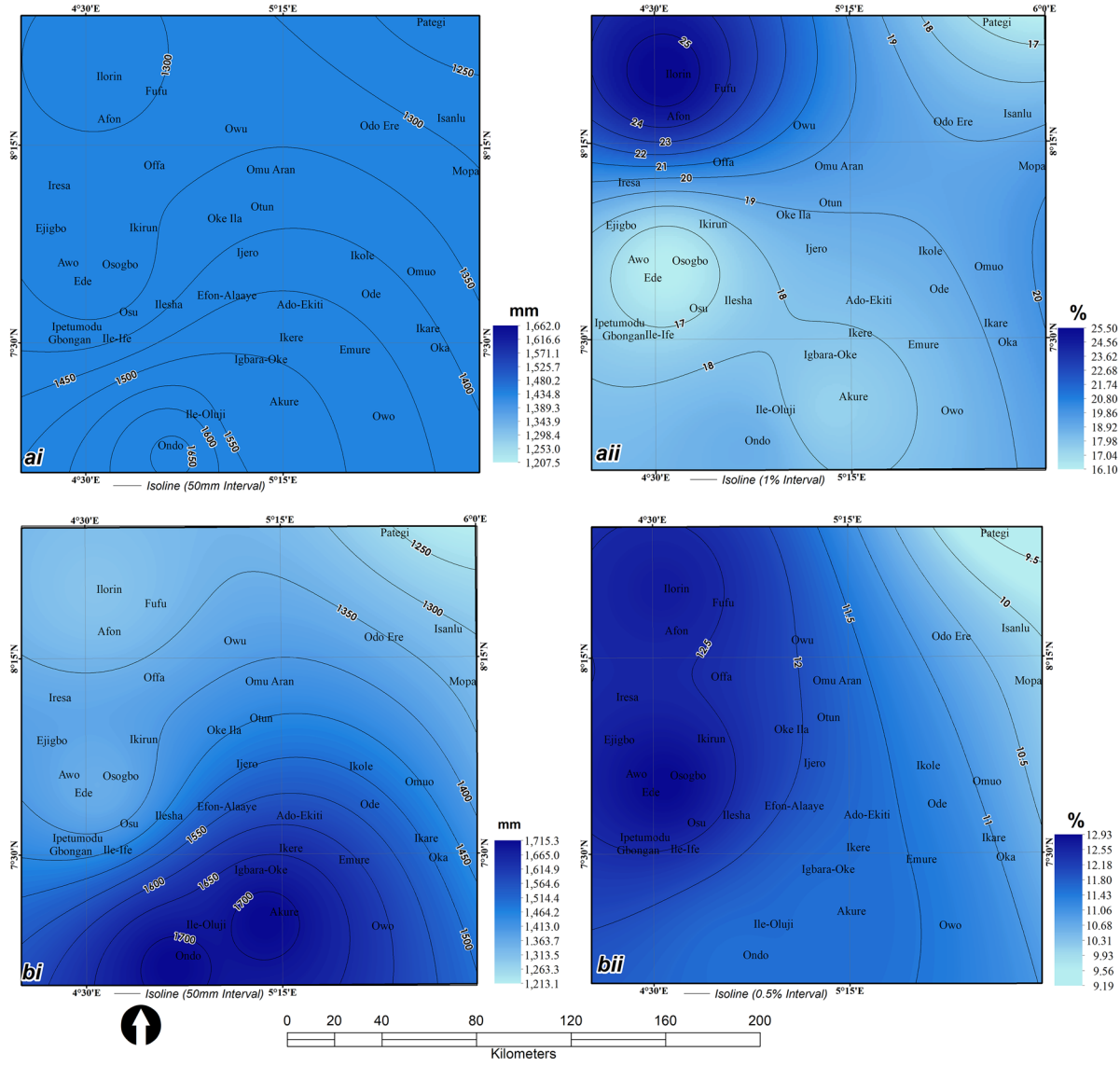

Fig. 6 Spatial patterns of the present (**ai** and **aii**) and future (**bi** and **bii**) rainfall variability

increased by about 61 km^2 from just 10.5 in 1972 to 72 km^2 in 2019, which represent about 582.5% expansion in its area extent. This is attributed to the massive dam construction during the period under study (Ayeni et al., 2013a, b, 2015, 2016). For instance, Asa, Ede, Egbe, Ejiba, Ero, and other dams were constructed during the period for both irrigation and domestic water supply. In addition, farmland gained about 32% between 1972 and 2019 from 5,430.5 to 7,156.6 km^2, respectively. However, there was a decline of agricultural activities between 1986 and 2002, thus, the study recorded a 48.4% drop in farmland. Meanwhile, it was recorded that the forest lost about 39% from 21,022 down to 12,823 km^2 within the period between 1972 and 2019 due to encroachment and degradation of forest, forest reserves, and protected area within the study area (Fasona et al., 2018). Again, the study revealed that forest lost 24% of its area extent between 2002 and 2019, while farmland and grassland gained about 87% and 5% within the same period, respectively. These are pointers to well-established indicators of deforestation and

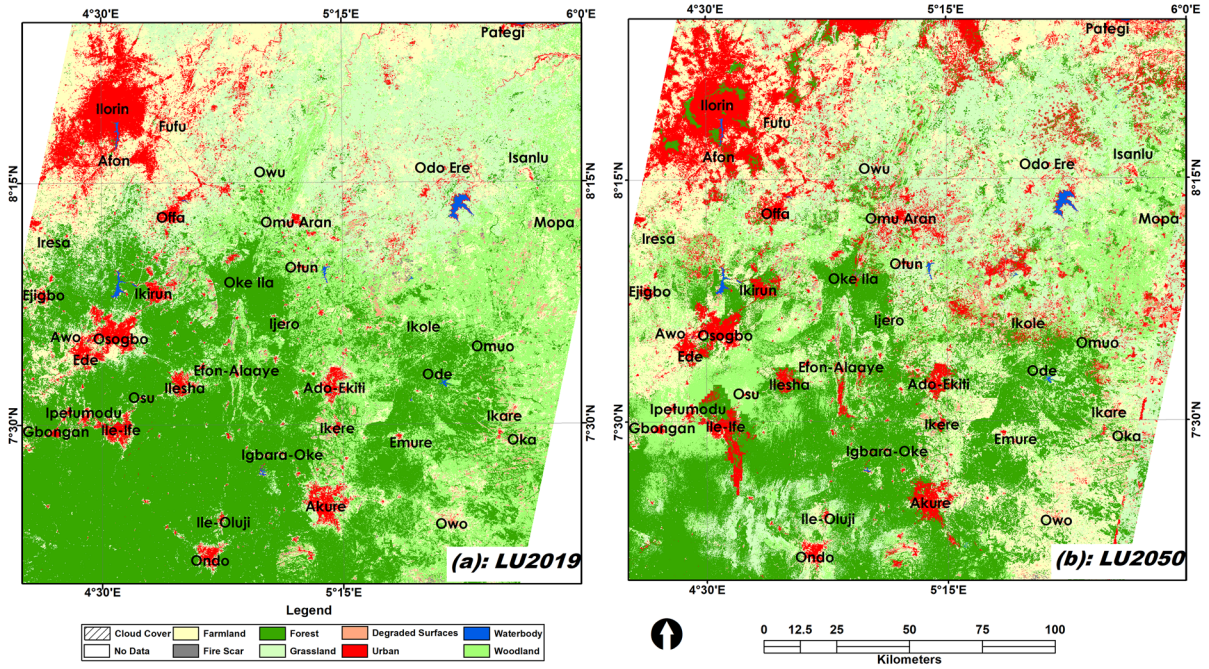

Fig. 7 Static characteristics of LULC during the **a** present and **b** future climates

forest degradation in the area. Between 2019 and 2050, however, forest and woodland were predicted to decrease to 28% and 21%. In addition, urban and woodland expanded by 103% and 31% between 2002 and 2019, while between 2002 and 2050, urban and woodland would increase by 302% and 4%, respectively.

Table 11 Static characteristics of the LULC, 2019 and 2050

LULC class	2019		2050	
	Area (km^2)	%	Area (km^2)	%
Cloud cover	0.0	0.0	0.0	0.0
Degraded surfaces	2,503.2	6.6	618.3	1.6
Farmland	4,180.9	11.1	8,738.4	23.1
Fire scar	471.0	1.2	123.2	0.3
Forest	17,334.1	45.9	9,147.4	24.2
Grassland	5,534.4	14.7	6,906.6	18.3
Area without data	2,774.6	7.3	2,007.1	5.3
Urban	1,631.4	4.3	4,372.3	11.6
Waterbody	97.1	0.3	77.2	0.2
Woodland	3,225.3	8.5	5,761.5	15.3
Total	37,751.9	100.0	37,751.9	100.0

Different practices for measuring LULCC can often produce substantial differences in resulting estimates of change. To illustrate this impact, we considered the results from a recent analysis implementing some of the recommended practices with that of a naïve, bi-temporal snapshot approach which does not (Badjana et al., 2017; Johnston, 2013; Laingen, 2015; Lark et al., 2015). The result showed that the intensity of climate induced deforestation and forest degradation will continue in the future, which accounts for about 99% and 22%, increase in urban area and agricultural expansion, while forest and woodland areas will lose about 29% and 21% of their area extent between 2019 and 2050, respectively. Finally, the study further predicted that the forested area would reduce with about 29% between 2019 and 2050 as against 60% of forest land that will be lost between 1972 and 2050. This confirmed the results of the previous studies predicted forest reduction (Badjana et al., 2017; Johnston, 2013; Wright et al., 2017). This is indication that the rate of forest degradation and deforestation will be more rapid than it was initially. In addition, other land use changes may have caused a subtle force of climate, preventing climate cooling might have been expected because of natural forcing

Table 12 Spatiotemporal characteristics of land use/land cover (2002–2050)

LULC class	LULC area extent (km^2)			Change in LULC (km^2)			% Change in LULC		
	2002	2019	2050	2002–2019	2002–2050	2019–2050	2002–2019	2002–2050	2019–2050
Cloud cover	0.0	0.0	0.0	0.0	0.0	0.0	0.0	0.0	0.0
Farmland	3,828.6	7,156.6	8,738.4	3,328.0	4,909.8	1,581.8	86.9	128.2	22.1
Degraded surface	1,479.1	402.8	618.3	−1,076.3	−860.8	215.5	−72.8	−58.2	53.5
Fire scar	539.8	105.7	123.2	−434.2	−416.6	17.5	−80.4	−77.2	16.6
Forest	16,959.5	12,823.1	9,147.4	−4,136.4	−7,812.2	−3,675.8	−24.4	−46.1	−28.7
Grassland	5,437.5	5,717.0	6,906.6	279.5	1,469.1	1,189.6	5.1	27.0	20.8
Area without data	2,783.7	2,007.1	2,007.1	−776.5	−776.5	0.0	−27.9	−27.9	0.0
Urban	1,087.4	2,202.0	4,372.3	1,114.6	3,284.9	2,170.3	102.5	302.1	98.6
Waterbody	77.0	71.9	77.2	−5.2	0.2	5.3	−6.7	0.2	7.4
Woodland	5,559.4	7,265.8	5,761.5	1,706.4	202.1	−1,504.3	30.7	3.6	−20.7
Total	**37,751.9**	**37,751.9**	**37,751.9**						

(Salinger, 2007; Kirtman et al., 2013; Li et al., 2015). While rainfall emerges as the dominant causative factor for the increase in vegetation greenness, there is an evidence of another causative factor, hypothetically a human-induced change superimposed on the climate trend (Huang & Kong, 2016; Shi et al., 2016; Tucker, 2005).

On the other hand, the study revealed that mean annual rainfall ranges between 1,208 and 1,662 mm across the study area and these extremes were recorded in Ondo and Pategi areas respectively during the present climate. Similar trend and direction have also been predicted for rainfall in Nigeria by other related studies in Nigeria (Odjugo, 2011; Seneviratne et al., 2010). The future climate (2020–2050), the spatial pattern of the mean annual rainfall, will show an increasing trend in north to south direction. It is predicted that within the study area, there will be more rainfall, between 1,213 and 1,715 mm, in the future climate. Similarly, Pategi and Ondo areas will receive highest and lowest mean annual rainfall. Climate change is increasing variability in rainfall and the shift increases uncertainty in crop production for humans and forage production (Messina et al., 2014; Tadross et al., 2009).

The study has shown that the annual rainfall variability indices range from 16 to 26% for the study area during the present climate, and Pategi and Akure recorded least and highest rainfall variability during the present climate. Also, annual rainfall was more stable in areas like Pategi, Oshogbo, Akure, and Ondo which recorded 15%, 16%, 17%, and 19% of rainfall variability index respectively than 25% recorded in and around Ilorin. Although the annual rainfall variability indices range from 9 to 13% for the study area, there will be a total shift in the distribution of rainfall variability indices in the future climate. Oshogbo and Ilorin will record highest rainfall variability index of 12.9% and 12.2% respectively and Pategi will receive 9.6%. This is consistent with the findings of Abiodun et al. (2012) and Bhowmik (2013).

The period of the rainy season in Nigeria has been reducing since 1941 when the onset and cessation were generally normal to 1971 when signals of late onset and early cessation of the rainy season set in (NIMET, 2012; Ogunrayi et al., 2016). Since then, the length of the rainy season has shrunken while annual total rainfall is about the same, thereby giving rise to high impact rainfall, resulting in flash floods (Tadross et al., 2009; NIMET, 2012; Ogunrayi et al., 2016; Rao et al., 2004; Sathiyamoorthy, 2005; Amekudzi et al., 2015). The upward trend in seasonal rainfall will have a more pronounced effect on agricultural activities in the area and influence the growth of crops with less irrigation requirement (Odjugo, 2011; Seneviratne et al., 2010). On the contrary, a downward trend in seasonal rainfall would have a more pronounced effect on agricultural activities (Ayeni et al., 2015; Sharma & Singh, 2017).

Many discussions have emerged on the notion of processes between LULC and climate changes on the globe. The current debate is on whether climate change actually exists and, if so, how it might be defined, measured, and assessed. This study

considered three contexts that explained the understanding of changes over time vis-à-vis understanding of climate variability; understanding of vegetation responses to perturbation; and understanding of social processes – human response to economic and political perturbation (Herrmann & Hutchinson, 2005). To better understand the interactions between climate and LULC, the reverse effects of LULC on climate mainly in terms of land use and land cover changes required continuous assessment. As observed, higher temperatures and, consequently, continuous cultivation enabled a decrease vegetation and major land use changes over the year. This is contrary to Briner et al. (2012), Schirpke et al. (2013), and Schirpke et al. (2017) where land cover changes were related to the expected natural reforestation of large previously abandoned grassland areas. These effects have resulted to environmental degradation including but not limited to land degradation, overgrazing, air pollution, forest and woodland clearing, and anthropogenic land disturbances (Salinger, 2007; Bullock et al., 1996; Sivakumar, 2007; Belaroui et al., 2014; Olagunju, 2015).

The analysis of the interaction between land use and climate systems at multiple scales requires conceptual frameworks and analytical methods to capture the complex and to accommodate temporal dynamics (Campbell, 1998; Ewel, 2001; Kinzig, 2001; Olson et al., 2008). The complexity of interactions has become challenging efforts to understand the linkages between land use and land cover change and land–atmosphere relationships and between ecological and societal processes over time and across space reflecting history, socio-economic conditions, and ecological circumstances as well as inherent in coupled human-natural systems (Kindermann et al., 2008; FAO, 2010; Rose et al., 2013; Zhang et al., 2014; Ostberg et al., 2015).

The combined impact of possible future changes resulting from interaction in land use and climate on landscapes remains debatable issues (Rose et al., 2013 and Ostberg et al., 2015) as LULC and climate changes are among the primary driving forces for terrestrial ecosystem (Kindermann et al., 2008; FAO, 2010; Zhang et al., 2014). Though this present study considered the importance of LULC and climate change with reference to rainfall, but the stabilization assessment of the impacts of temperature on the totality of the environment can not be underestimated. Therefore, the bounded continuum of rainfall and temperature should be taken into account for such land-based climate interaction assessment in order to predict spatiotemporal climatic trend with acceptable accuracy (Kindermann et al., 2008; FAO, 2010; Rose et al., 2013; Ostberg et al., 2015; Bhowmik, 2012).

Conclusion

This study evaluated the coupled interaction of land use/land cover and climate change in the derived savannah zone of Nigeria by determining the extent, magnitude, direction, and location of LULCC (1972–2019). Also, it assessed the climate variability for the period between 1941 and 2019 and predicted the interaction of LULC and climate change during future climate (2020–2050) through LCM technique. The research concluded that climate change and variability within the derived savannah ecological zone of Nigeria has been transformed to an extent that it has effects on spatial pattern and distribution of LULC within the area. In addition, the study confirmed the spatial pattern and trend for the zone in which rainfall will continue to increase in a north-southward direction and affirmed the latitudinal characteristics of rainfall with the lowest in Pategi, northern part of the study area. Furthermore, the study revealed that climate is one main underlying driver of LULCC. The interaction between the LULC and climate change has led to the uncontrollable processes of deforestation and forest degradation within the study area.

Acknowledgements The authors gratefully acknowledged Department of Geography, University of Lagos, Nigeria.

Availability of data and material There are no external data used in this research.

Code availability Not applicable.

Declarations

Conflict of interest The authors declare no competing interests.

References

Abiodun, B. J., Lawal, K. A., Salami, A. T., & Abatan, A. A. (2012). Potential influences of global warming on future climate and extreme events in Nigeria. *Regional Environmental Change*, 1-15. https://doi.org/10.1007/s10113-012-0381-7

Akinsanola, A. A., & Ogunjobi, K. O. (2014). Analysis of rainfall and temperature variability over Nigeria. *Global Journal of Human-Social Science: B Geography, Geo-Sciences, Environmental Disaster Management, 14*(3), 1–17.

Amekudzi, L. K., Yamba, E. I., Ernest, K. P., Asare, O., Aryee, J., Baidu, M., & Codjoe, S. N. A. (2015). Variabilities in rainfall onset, cessation and length of rainy season for the various agro-ecological zones of Ghana. *Climate, 3*, 416–434. https://doi.org/10.3390/cli3020416

Armenteras, D., Gibbes, C., Vivacqua, C. A., Espinosa, J. S., Duleba, W., Goncalves, F., & Castro, C. (2016). Interactions between climate, land use and vegetation fire occurrences in El Salvador. *Atmosphere*, 7(26). https://doi.org/10.3390/atmos7020026

Armston, J. D., Danaher, T. J., Goulevitch, B. M., & Byrne, M. I. (2002). Geometric correction of Landsat MSS, TM, and ETM+ imagery for mapping of woody vegetation cover and change detection in Queensland. In: *Proc. 11th Australasian Remote Sensing and Photogrammetry Conference*, Brisbane.

Ayeni A. O., Cho, M. A., Ramoelo, A., Mathieu, R., Soneye, A. S. O., & Adegoke, J. O. (2013). Could local perceptions of water stress be explained by LULCC? *Geoinfor Geostat: An Overview,* S1. https://doi.org/10.4172/2327-4581.S1-001

Ayeni A., Kapangaziwiri, E., Soneye, A., Vezhapparambu, S. & Adegoke, J. (2013). Assessing the impact of land use/land cover and climate changes on water stress in the derived savanna. In: In Eva Bogh et al. (eds), *Climate and land surface changes in hydrology*. Proceedings of H01, IAHS-IAPSO-IASPEI Assembly, Gothenburg, Sweden, July 2013. IAHS Publ. 359, 92–98. ISBN Number: 978–1–907161–37–7.

Ayeni, A. O., Kapangaziwiri, E., Soneye, A. S. O., & Engelbrecht, F. (2015). Assessing the impact of global changes on the surface water resources of Southwestern Nigeria. *Hydrological Sciences Journal (HSJ), 60*(11 & 12), 1956–1971.

Ayeni, A. O., Cho, M. A., Mathieu, R., & Adegoke, J. O. (2016). The local experts' perception of environmental change and its impacts on surface water in Southwestern Nigeria. *Environmental Development, 17*, 33–47.

Badjana, H. M., Olofsson, P., Woodcock, C., Helmschrot, E. J., Wala, K. P., & Akpagan, K. (2017). Mapping and estimating land change between 2001 and 2013 in a heterogeneous landscape in West Africa: Loss of forestlands and capacity building opportunities. *International Journal of Applied Earth Observation and Geoinformation, 63*, 15–23.

Belaroui, K., Djediai, H., & Megdad, H. (2014). The influence of soil, hydrology, vegetation and climate on desertification in El-Bayadh region (Algeria). *Desalination and Water Treatment, 52*(10–12), 2144–2150.

Bhowmik, A. K. (2012). A comparison of Bangladesh climate surfaces from the geostatistical point of view. *ISRN Meteorology*. https://doi.org/10.5402/2012/353408

Bhowmik, A. K. (2013). Temporal patterns of the two-dimensional spatial trends in summer temperature and monsoon precipitation of Bangladesh. *ISRN Atmospheric Sciences*. https://doi.org/10.1155/2013/148538

Bowman, D. M., Balch, J. K., Artaxo, P., Bond, W. J., Carlson, J. M., Cochrane, M. A., & Pyne, S. J. (2009). Fires in the earth system. *Science, 324*, 481–484.

Briner, S., Elkin, C., Huber, R., & Grêt-Regamey, A. (2012). Assessing the impacts of economic and climate changes on land-use in mountain regions: A spatial dynamic modeling approach. *Agriculture, Ecosystems & Environment, 149*, 50–63.

Bullock, P., Le Houerou, H., Hoffman, M. T., Rounsevell, M., Sehgal, J., Varallyay, G., Aidoud, A., Balling, R., Long-Jun, C., & Goulding, K. W. T. (1996). Land degradation and desertification. In R. T. Watson, R. H. Moss, & M. C. Zinyowera (Eds.), *Climate change 1995. Impacts, adaptations and mitigation of climate change: Scientific and technical analyses.* Cambridge University Press (CUP) Cambridge. pp. 173–189

Campbell, D. J. (1998). Towards an analytical framework for land use change. In L. Bergstrom & H. Kirschmann (Eds.), *Carbon and nutrient dynamics in natural and tropical agricultural ecosystems* (pp. 281–301). CAB International.

Campbell, J. B. & Wynne, R. H. (2011). *Introduction to remote sensing* (5th edition, pp.667.). New York: The Guilford Press.

Cook, K. H., & Vizy, E. K. (2006). Coupled model simulations of the West African monsoon system: Twentieth- and twenty-first-century simulations. *Journal of Climate, 19*, 3681–3703.

Dale, V. H. (1997). The relationship between land use change and climate change: Ecological applications. *Ecological Society of America, 7*(3), 753–769.

de Vries, C., Danaher, T., Denham, R., Scarth, P., & Phinn, S. (2007). An operational radiometric calibration procedure for the Landsat sensors based on pseudo invariant target sites. *Remote Sensing of Environment, 107*(3), 414–429.

Deng, X., Zhao, C., & Yan H. (2013), Systematic modeling of impacts of land use and land cover changes on regional climate: A review. *Advances in Meteorology*, 1–11. https://doi.org/10.1155/2013/317678

Eastman, J. R. & Laney, R. M. (2002). Bayesian soft classification for sub-pixel analysis: A critical evaluation. *Photogrammetric Engineering and Remote Sensing*, *68*(11), 1149 – 1154.

Eastman, R. (2012). *IDRISI Selva manual guide to GIS and image processing* (17, Pp 332). Worcester, MA, USA: Clark University.

Ewel, K. C. (2001). Natural resource management: The need for interdisciplinary collaboration. *Ecosystems, 4*, 716–722.

Fan, X., Ma, Z., Yang, Q., Han, Y., & Mahmood, R. (2015). Land use/land cover changes and regional climate over the loess plateau during 2001–2009, Part II: Interrelationship from observations. *Climate Change, 129*(3), 441–455. https://doi.org/10.1007/s10584-014-1068-5fv

FAO. (2010). *Global forest resources assessment 2010: Main report*. Food and Agriculture Organization of the United Nations.

Fasona, M. J., Akintuyi, A. O., Udofia, S. K., Akoso, T. M., Ariori, A. N., Adeonipekun, P. A., Agboola, O. O., Ogunsanwo, G. E., Ogundipe, O. T., Soneye, A. O., & Omojola, A. S. (2018). Deforestation and land-cover changes in forest reserves of Southwest, Nigeria. *Lagos Journal of Geo-Information Sciences (LJGIS), 5*, 67–87.

Fasona, M.J., & Omojola, A.S. (2005). Climate change, human security and communal clashes in Nigeria. *Proceeding of*

International Workshop on Human Security and Climate Change, Holmen Fjord Hotel, Asker, near Oslo, 22–23 June 2005. Accessed on 10 Aug 2007, Retrieved from: www.gechs.org/activities/holmen/Fasona_Omojola.pdf

Federal Ministry of Environment (FME). (2004). *National biodiversity strategy and action plan* (pp 1–144). Abuja-Nigeria: FME.

Fisher, B., Turner, R. K., & Morling, P. (2009). Defining and classifying ecosystem services for decision making. *Ecological Economics, 68*, 643–653.

Geist, H. J., & Lambin, E. F. (2004). Dynamic causal patterns of desertification. *BioScience, 54*(9), 817–829.

Herrmann, S. M., & Hutchinson, C. F. (2005). The changing contexts of the desertification debate. *Journal of Arid Environments, 63*(3), 538–555.

Hewitson, B. C., & Crane, R. G. (1996). Climate downscaling: Techniques and application. *Climate Research, 7*, 85–95.

Huang, S., & Kong, J. (2016). Assessing land degradation dynamics and distinguishing human-induced changes from climate factors in the Three-North Shelter forest region of China. *ISPRS International Journal of Geo-Information, 5*, 158. https://doi.org/10.3390/ijgi5090158

Johnston, C. A. (2013). Wetland losses due to row crop expansion in the Dakota Prairie Pothole region. *Wetlands, 33*, 175–182.

Kindermann, G., Obersteiner, M., Sohngen, B., Sathaye, J., Andrasko, K., Rametsteiner, E., et al. (2008). Global cost estimates of reducing carbon emissions through avoided deforestation. *Proceedings of the National Academy of Sciences U. S. A., 105*(30), 10302–10307.

Kinzig, A. P. (2001). Bridging disciplinary divides to address environmental and intellectual challenges. *Ecosystems, 4*, 709–715.

Kirtiloglu, O. S., Orhan, O., & Ekercin, S. (2016). A map mash-up application: Investigation the temporal effects of climate change on Salt Lake Basin. *ISPRS International Archives of the Photogrammetry, Remote Sensing and Spatial Information Sciences*, XLI-B4, 221-2260. https://doi.org/10.5194/isprs-archives-XLI-B4-221-2016

Kirtman, B., Power, S. B., Adedoyin, J. A., Boer, G. J., Bojariu, R., Camilloni, I., Doblas-Reyes, F. J., Fiore, A. M., M. Kimoto, M., Meehl, G. A., Prather, M., Sarr, A., Schär, C., Sutton, R., van Oldenborgh, G. J., Vecchi, G., & Wang, H. I. (2013). Near-term climate change: Projections and predictability. In T. F. Stocker, et al. (Eds.), *Climate change 2013: The physical science basis. Contribution of Working Group I to the Fifth Assessment Report of the Intergovernmental Panel on Climate Change*, Cambridge, UK: Cambridge University Press.

Laingen, C. (2015). Measuring cropland change: A cautionary tale. *Papers in Applied Geography, 1*(1), 65–72. https://doi.org/10.1080/23754931.2015.1009305

Lark, T. J., Salmon, J. M., & Gibbs, H. K., (2015). Cropland expansion outpaces agricultural and biofuel policies in the United States. *Environmetal Research Letter, 10*(4), https://doi.org/10.1088/1748-9326/10/4/044003

Lark, T. L., Mueller, R. M., Johnson, D. M., & Gibbs, H. K. (2017). Measuring land-use and land-cover change using the U.S. department of agriculture's cropland data layer: Cautions and recommendations. *International Journal of Applied Earth Observation and Geoinformation, 62*, 224–235.

Li, Z., Deng, X., Yin, F., & Yang, C. (2015). Analysis of climate and land use changes impacts on land degradation in the North China Plain. *Advances in Meteorology*. https://doi.org/10.1155/2015/976370

Matthews, E. (1983). Global vegetation and land use: New high resolution data bases for climate studies. *Journal of Climate and Applied Meteorology, 22*, 474–487.

Meehl, G. A., Covey, C., McAvaney, B., Latif, M., & Stouffer, R. J. (2005). Overview of the coupled model intercomparison project. *Bulletin of the American Meteorological Society, 86*, 89–93.

Messina, J., Adhikari, U., Carroll, J., Chikowo, R., DeVisser, M., Dodge, L., Fan, P., Langley, S., Lin, S., Mensope, N., Moore, N., Murray, S., Nawyn, S., Nejadhashemi, A. Olson, J., Smith, A., & Snapp, S. (2014). *Population growth, climate change and pressure on the land – Eastern and Southern Africa*, 99pp. ISBN 978 – 0–9903005–0–2

Mutiibwa, D., Kilic, A., & Irmak, S. (2014). The effect of land cover/land use changes on the regional climate of the USA high plains. *Climate, 2*(3), 153–167. http://www.mdpi.com/journal/climate

National Bureau of Statistics (NBS). (2006). Federal Republic of Nigeria: 2006 population census. Pp10. http://www.nigerianstat.gov.ng

NIMET. (2012). Nigerian climate review edit. Nigerian Meteorological Agency (NIMET) http://www.nimet.gov.ng/sites/default/files/publications/2012%20NIGERIAN%20CLIMATE%20REVIEW%20EDIT.docx

Odjugo, P. A. O. (2011). Climate change: Evidence, impacts and adaptation strategies in Nigeria. In A. T. Salami & O. I. Orimoogunje (Eds.), *Environmental research and challenges of sustainable development in Nigeria* (pp. 142–164). Obafemi Awolowo University Press.

Ogunrayi, O. A., Akinseye, F. M., Goldberg, V., & Bernhofer, C. (2016). Descriptive analysis of rainfall and temperature trends over Akure Nigeria. *Journal of Geography and Regional Planning, 9*(11), 195–202.

Oguntunde, P. G., Abiodun, B. J., Gunnar, & L,. (2011). Rainfall trends in Nigeria, 1901–2000. *Journal of Hydrology, 411*, 207–218. https://doi.org/10.1016/j.jhydrol.2011.09.037

Oguntunde, P. G., Abiodun, B. J., & Gunnar, L. (2012). Spatial and temporal temperature trends in Nigeria, 1901–2000. *Meteorology and Atmospheric Physics, 118*, 95–105.

Olagunju, T. E. (2015). Drought, desertification and the Nigerian environment: A review. *Journal of Ecology and the Natural Environment, 7*(7), 196–209.

Oliver, T. H., & Morecroft, M. D. (2014). Interactions between climate change and land use change on biodiversity: Attribution problems, risks, and opportunities. *Wires Climate Change, 5*, 317–335. https://doi.org/10.1002/wcc.271

Olson, J. M., Alagarswamy, G., Andresen, J. A., Campbell, D. J., Davis, A. Y., Gef, J., Huebner, M., Lofgren, B. M., Lusch, D. P., Moore, N. J., Pijanowski, B. C., Qi, J., Thornton, P. K., Torbick, N. M., & Wang, J. (2008). Integrating diverse methods to understand climate–land interactions in East Africa. *Geoforum, 39*, 898–911.

Omotoso, F. (2009). Administrative problems of state creation in Ekiti State, Nigeria. *African Journal of Political Science and International Relations*, *3*(3), 107–116. Retrieved from http://www.academicjournals.org/article/article1379786015_Omotosho.pdf

Orhan, O., Ekercin, S., & Dadaser-Celik, F. (2014). Use of Landsat land surface temperature and vegetation indices for monitoring

drought in the Salt Lake Basin Area, Turkey. *The Scientific World Journal*, 2014. https://doi.org/10.1155/2014/142939

Ostberg, S., Schaphoff, S., Lucht, W., & Gerten, D. (2015). Three centuries of dual pressure from land use and climate change on the biosphere. *Environmental Research Letter*, *10*, 044011.

Pielke, R. A., Sr., Adegoke, J., Beltran-Przekurat, A., Hiemstra, C. A., Lin, J., Nair, U. S., & Nobis, T. E. (2007). An overview of regional land-use and land-cover impacts on rainfall. *Tellus, 59B*, 587–601.

Pielke, R. A. (1997). The role of land cover as a driving for regional climate change. In S.J. Hassol, & J. Katzenberger (Eds.), *Scaling from site-specific observations to global model grids* (pp.89–92). Proceeding of an Aspen Global Change Institute Workshop 7–17 July 1997, Elements of Change series, AGCI.

Pielke, R. A., & Avissar, R. (1990). Influence of landscape structure on local and regional climate. *Landscape Ecology, 4*(2–3), 133–155.

Pitman, A., Pielke, R., Sr., Avissar, R., Claussen, M., Gash, J., & Dolman, H. (2000). The role of the land surface in weather and climate: Does the land surface matter? *IGBP Newsletter, 39*, 4–11.

Pontius, R. G., Jr. (2000). Quantification error versus location error in comparison of categorical maps. *Photogrammetric Engineering and Remote Sensing, 66*(8), 1011–1016.

Rao, B., & D. Rao D., & Rao, V. B. (2004). Decreasing trend in the strength of tropical easterly jet during the Asian summer monsoon season and the number of tropical cyclonic systems over Bay of Bengal. *Geophysical Research Letters, 31*, L14103.

Rose, S. K., Kriegler, E., Bibas, R., Calvin, K., Popp, A., van Vuuren, D. P., & Weyant, J. (2013). Bioenergy in energy transformation and climate management. *Climate Change, 123*(4), 77–93.

Salinger, M. J. (2007). Agriculture's influence on climate during the Holocene. *Agricultural and Forest Meteorology, 142*(2–4), 96–102.

Sathiyamoorthy, V. (2005). Large scale reduction in the size of the tropical easterly jet. *Geophysical Research Letters, 2005*, 32.

Schirpke, U., Leitinger, G., Tasser, E., Schermer, M., Steinbacher, M., & Tappeiner, U. (2013). Multiple ecosystem services of a changing Alpine landscape: Past, present and future. *Int. J. Biodivers. Sci. Ecosystem Services Management, 9*, 123–135.

Schirpke, U., Kohler, M., Leitinger, G., Fontana, V., Tasser, E., & U. Tappeiner, U. (2017). Future impacts of changing land-use and climate on ecosystem services of mountain grassland and their resilience. *Ecosystem Services*, *26*(A), 79–94.

Seneviratne, S. I., Corti, T., Davin, E. L., Hirschi, M., Jaeger, E. B., Lehner, I., Orlowsky, B., & Teuling, A. J. (2010). Investigating soil moisture–climate interactions in a changing climate. *Earth-Science Reviews, 99*(3–4), 125–161.

Sharma, S. & Singh, P. K. (2017). Long term spatiotemporal variability in rainfall trends over the state of Jharkhand, India. *Climate, 5*, 18. https://doi.org/10.3390/cli5010018

Shi, X., Wang, W., & Shi, W. (2016). Progress on quantitative assessment of the impacts of climate change and human activities on cropland change. *Journal of Geographical Sciences, 26*(3), 339–354.

Sivakumar, M. V. K. (2007). Interactions between climate and desertification. *Agricultural and Forest Meteorology, 142*(2–4), 143–155.

Smith, M. J., Goodchild, M. F., & Longley, P. A. (2007). Geospatial analysis: Comprehensive guide to principles, techniques and software tools (2nd edition). https://doi.org/10.1111/j.1467-9671.2008.01122.x

Sohl, T. L., Sleeter, B. M., Sayler, K. L., Bouchard, M. A., Reker, R. R., Bennett, S. L., Sleeter, R. R., Kanengieter, R. L., & Zhu, Z. (2012). Spatially explicit land-use and land-cover scenarios for the Great Plains of the United States. *Agriculture, Ecosystems and Environment, 153*, 1–15.

Tadross, M., Suarez, P., Lotsch, A., Hachigonta, S., Mdoka, M., Unganai, L., et al. (2009). Growing-season rainfall and scenarios of future change in southeast Africa: Implications for cultivating maize. *Climate Research, 40,* 147–161.

Tucker, C. J. (2005). Recent trends in vegetation dynamics in the African Sahel and their relationship to climate. *Global Environmental Change, 15*(4), 394–404.

Tucker, C. J., Grant, D. M., & Dykstra, J. D. (2004). NASA's global orthorectified Landsat data set. *Photogrammetric Engineering & Remote Sensing, 70*(3), 313–322.

Wang, Y., Woodcock, C. E., Buermann, W., Stenberg, P., Voipio, P., Smolander, H., et al. (2004). Evaluation of the MODIS LAI algorithm at a coniferous forest site in Finland. *Remote Sensing of Environment, 91*, 114–127.

Wang, S., & Davidson, A. (2007). Impact of climate variations on surface albedo of a temperate grassland. *Agricultural and Forest Meteorology, 142*(2–4), 133–142.

Wright, C. K., Larson, B., Lark, T. J., & Gibbs, H. K. (2017). Recent grassland losses are concentrated around U.S. ethanol refineries. *Environmental Research Letter, 12*(4), 044001. https://doi.org/10.1088/1748-9326/aa6446

Wright, C. K., Wimberly, M. C., et al. (2013). Reply to Kline: Cropland data layer provides a valid assessment of recent grassland conversion in the Western Corn Belt. *Proceedings of the National Academy of Sciences, 110*(31), E2864. https://doi.org/10.1073/pnas.1307594110

Xiong, X., Grunwald, S., Myers, D. B., Ross, C. W., Harris, W. G., & Comerford, N. B. (2014). Interaction effects of climate and land use/land cover change on soil organic carbon sequestration. *Science of the Total Environment, 493*, 974–982.

Yaqian He, Y., Timothy, A., Warner, T. A., McNeil, B. E., & Lee, E. (2018). Reducing uncertainties in applying remotely sensed land use and land cover maps in land-atmosphere interaction: Identifying change in space and time. *Remote Sensing, 10*(4), 506. https://doi.org/10.3390/rs10040506.

Zeng, N., Neelin, J. D., Lau, K. M., & Tucker, C. J. (1999). Enhancement of interdecadal climate variability in the Sahel by vegetation interaction. *Science, 286*, 1537–1540.

Zhang, Y., Song, C., Zhang, K., Cheng, X., Band, L. E., & Zhang, Q. (2014). Effects of land use/land cover and climate changes on terrestrial net primary productivity in the Yangtze River Basin, China, from 2001 to 2010. *Journal of Geophysical Research. Biogeosciences, 119*, 1092–1109.

Zheng, X., & Eltahir, E. A. B. (1997). The response to deforestation and desertification in a model of West African Monsoons. *Geophysical Research Letters, 24*(2), 155–158.